Underpotential deposition of SnBi thin films for sodium ion batteries: The effect of deposition potential and Sn concentration

Nqobile Xaba [a, b], Remegia M. Modibedi [a, *], Lindiwe E. Khotseng [b], Mkhulu K. Mathe [a], Nithyadharseni Palaniyandy [a]

[a] Energy Materials, Energy Centre, Council for Scientific and Industrial Research (CSIR), 11 Meiring Naudé Road, Pretoria, 0001, South Africa
[b] Department of Chemistry, University of Western Cape, Private Bag X17, Bellville, 7535, South Africa

ARTICLE INFO

ABSTRACT

Bimetallic SnBi film was deposited on a Cu foil substrate via the electrochemical atomic layer deposition (E-ALD) technique. The deposition attainment of Sn and Bi were investigated using cyclic voltammetry (CV) and linear sweep voltammetry (LSV). The deposition potential of Bi was varied in the underpotential deposition (UPD) region and the concentration of Sn was varied in the SnBi bimetallic material. The materials were characterised using field emission scanning electron microscopy coupled with energy dispersive spectroscopy (FE-SEM/EDS) for morphology and elemental distribution, focused ion beam scanning electron microscopy (FIBSEM) for thickness, X-ray diffraction (XRD) for crystallinity and inductively coupled plasma mass spectroscopy (ICP-MS) for composition measurements. Bi deposited at different UPD regions was structurally different. The deposits were crystalline SnBi materials containing Sn, Bi and other phases of Cu and Sn. Bi was concentrated on the surface, while Sn was distributed evenly across the film. The SnBi electrodes were tested as anode materials in Na-ion batteries using galvano-static cycling (GC), CV and electrochemical impedance spectroscopy (EIS). Initial discharge capacities of 1900 mAh g^{-1} for SnBi (1:1) and 341 mAh g^{-1} for SnBi (3:1) electrodes at 38.5 mA g^{-1} were obtained, while the electrodes suffered capacity loss after 10 cycles.

© 2019 Elsevier B.V. All rights reserved.

1. Introduction

The development of thin film materials is of critical importance in today's technology. Thin film material applications are found in electronic components, photonics, sensors as well as in energy conversion and storage [1]. Alloy materials of Sn and Bi are essential components in interconnecting and packaging electronic constituents [2]. The use of Bi as Pb replacement in Sn–Pb alloys was motivated by the quest for environmentally friendly materials that would result in the reduction of toxic Pb-based materials. Alloys of Sn and Bi have of late found renewed interest as anode materials for rechargeable sodium ion batteries [3]. This is due to their high theoretical capacity, where Bi has a capacity of 385 mAh g^{-1} and Sn that of 847 mAh g^{-1} [4,5]. Their use is limited by the large volumetric expansion of the electrode during cycling, causing capacity loss, and research in this area is focused on material development

[6–8].

Different techniques are reported in literature, focusing on the preparation of alloy materials for electronic components, which amongst others include vacuum evaporation, screen-printing, electroplating, sonochemistry, hydrothermal synthesis and the solid-state method [9–12]. Electrodeposition is the widely used method because it is versatile, simple and cheap [10]. SnBi materials on various copper substrates have been previously prepared using electrodeposition methods. They were electrodeposited from a bath using pulse deposition onto planar Cu sheets [13], electrodeposited with complexing agents onto Cu/Ni plates [14], electrolessly deposited onto Cu foil [15] and from a deep eutectic solvent onto Cu foil [10]. These methods use complexing agents and additives, including methane sulfonic acid (MSA), ethylenediaminetetraacetic acid (EDTA), polyethylene glycol (PEG), gelatin, choline chloride ethylene glycol (CCEG) and H$_3$BO$_3$. Complexing agents and additives supress the formation of dendrite structure and concurrently reduce the difference in potentials of the deposited elements.

The chemistry of SnBi deposition process involves codeposition

of SnBi forming a wide range of alloys. Bi standard reduction potential (Equation (1)) is approximately 0.45 V more positive than that of Sn (Equation (2)). This potential difference allows for the co-deposition of SnBi and also the deposition can be selectively turned on and off for the deposition of Sn [13].

$$Bi^{3+} + 3e^- \rightarrow Bi \quad (+0.317V) \tag{1}$$

$$Sn^{2+} + 2e^- \rightarrow Sn \quad (-0.137V) \tag{2}$$
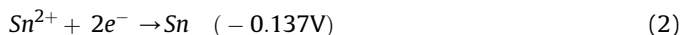
E-ALD is an attractive process to prepare thin film materials. This process is derived from atomic layer deposition and electrochemical epitaxy developed by Gregory and Stickney [16]. It involves layer-by-layer growth of atomic layers of elements in a cycle to form a compound using surface-limited redox reactions (SLRR) and UPD. UPD refers to the deposition of the atomic layer of an element onto another element at a potential under that required to deposit the element on itself. E-ALD has been used to make compounds of II-IV elements, including HgSe [17], CdTe [18], CdS [19], PdSe, PbTe [20], CuInSe$_2$ [21], Ge$_x$Sb$_y$Te$_z$ [22], In$_2$Se$_3$ [23], Cu$_2$Se [24], Bi$_2$Te$_3$ [25], Pt, Pd-based electrocatalysts including Pd nanofilms [26], Pt nanofilms [27] and Pt−Ru [28,29].

This study reports on the preparation of SnBi thin films using the E-ALD technique without additives. In addition, we report on their use as binder-free electrode materials for Na-ion batteries. SnBi alloys were deposited on Cu foil substrates from aqueous solutions of SnCl$_2$ and BiCl$_3$ in HCl electrolyte. CV and LSV were used to study the oxidation and reduction of each precursor solution for the development of the deposition process. The morphological features, thickness and crystalline phases of the prepared SnBi films were investigated using FE-SEM, FIB-SEM and XRD, respectively. EDS was used for the surface elemental mapping and compositional analysis was done using ICP-MS. The electrochemical performance of SnBi films for Na-ion batteries was evaluated using GC, CV and EIS, respectively.

2. Experimental synthesis and characterisation techniques

2.1. Chemicals, solutions and substrate

The chemical solutions used were 1 mM SnCl$_2$ (Sigma Aldrich), 1 mM BiCl$_3$ (Sigma Aldrich) and 0.5 M HCl (32%, Associated Chemical Enterprise) as the electrolyte. A concentration range of 0.1 mM, 0.2 mM, 0.4 mM, 0.6 mM and 0.8 mM SnCl$_2$ solutions in 0.1 M HCl was used as well as a 0.2 mM BiCl$_3$ solution. All solutions were prepared in an electrolyte solution. ACS reagent grade chemicals and high purity ($\leq$1 μS/cm) and deionised water were used. The resultant pH of the solutions was 2.3. Cu foil (99%, 9 μm, Gelon) was used as a substrate. The copper foil was cleaned with dilute nitric acid (5 wt %), then rinsed with deionised water, subsequently dipped in acetone and finally air-dried.

2.2. Synthesis method

Electrodeposition of SnBi was carried out placing the prepared Cu foil substrate in the electrochemical flow cell. The substrate cleaning cycle began by pumping the electrolyte solution into the cell. The potential of the cell was alternated/cycled three times between −0.050 V − (−0.50 V) to further clean the Cu substrate. The electrochemical cell used consisted of an auxiliary Au wire electrode, Ag/AgCl (3 M KCl) (MF-2021, BASi) reference electrode and the Cu foil as the working electrode. Degassed solutions (N$_2$, 1 h) were pumped into the cell through master flex tubes from their reservoirs using a peristaltic pump. The solutions were contained

within a deposition area of 2.1 cm^2 in the flow cell using a rubber gasket. The scan rate used for all experiments was 10 mV s^{-1}. The deposition parameters of SnBi on Cu foil method were developed using CV (PGSTAT101) equipped with NOVA 1.8 software and potential or current versus time plots were generated from Sequencer 4 software.

2.3. Material characterisation

Field emission scanning electron microscopy was performed using a LEO 1525 FE-SEM with the acceleration voltage of 2.00 kV and EDS for elemental mapping. Cross-sectional scanning electron microscope imaging was done by fracturing the sample in liquid nitrogen and placing the fractured edge facing up on the stub. The samples were viewed with a ZEISS Auriga FIB-SEM using martSEN software version V05.04.00. The EDS was done using the Oxford X-Men detector and Aztec software. XRD was performed on the Rigaku Ultima IV X-ray diffractometer with a monochromatised Cu Kα radiation of $\lambda = 1.5406$ Å at the 2θ range of 10−90°. The spectra were matched and refined using HighScore Plus software and PDF 4 FILE 2017. Quantitative analysis was performed using Thermo Scientific iCAP Q ICP-MS equipped with Qtegra Intelligent Scientific Data Solution software.

2.4. Electrochemical characterisation

The synthesised SnBi films were tested as anode materials for Na-ion batteries using 2032-type coin cells. The cell components included Na disc as counter electrode and 1 M NaClO$_4$ in ethylene carbonate-diethylene carbonate (EC: DEC, 50:50 vol %) solution as electrolytes, and a glass microfiber (Whatman GF/F) was used as a separator. The coin cells were assembled in an Ar-filled glove box (MBraun MB 150B-G, Germany, maintaining the concentrations of O$_2$ and H$_2$O < 1 ppm). The cells were characterised by GC, CV and EIS. The GC was analysed using a MACCOR Series 4000 tester. CV and EIS were performed on a Bio-Logic VMP3 potentiostat/galvanostat controlled by EC-Lab v10.40 software at the scan rate of 0.1 mV s^{-1} with the potential range of 0.005−3.0 V. The EIS plots were recorded by applying 10 mV amplitude over the frequency range from 100 kHz to 10 mHz at room temperature and the data were analysed using Z-view software (version 2.2, Scribner Assoc., Inc., USA).

3. Results and discussion

3.1. Preparation of SnBi and Bi thin film electrodes

Microstructured SnBi thin films were prepared on Cu foil by first studying individually the electrochemistry of Sn and Bi on Cu foil substrate using CV. The acquired information was then used to formulate a deposition cycle used to deposit the material.

3.1.1. Electrochemical studies: cyclic voltammetry

Fig. 1(a) and (b) inserts show a cyclic voltammogram of a Cu foil substrate in a 0.1 M HCl solution. All the scans were started on the positive mode and scanned towards the negative limit and then reversed. The CV demonstrated that the initial open circuit potential was at −0.05 V, a reduction peak of Cu oxides at −0.1 V (A) and hydrogen evolution occurred beyond −0.5 V. Stickney and Ehlers [30] found a similar outcome from a study of Cu (111) electrodes in an aqueous HCl solution. They concluded that the copper oxide layer dissolves when the substrate is immersed in the solution and then replaced by a copper chloride monolayer, resulting in a change in the initial potential from −0.05 V to approximately −0.12 V. The
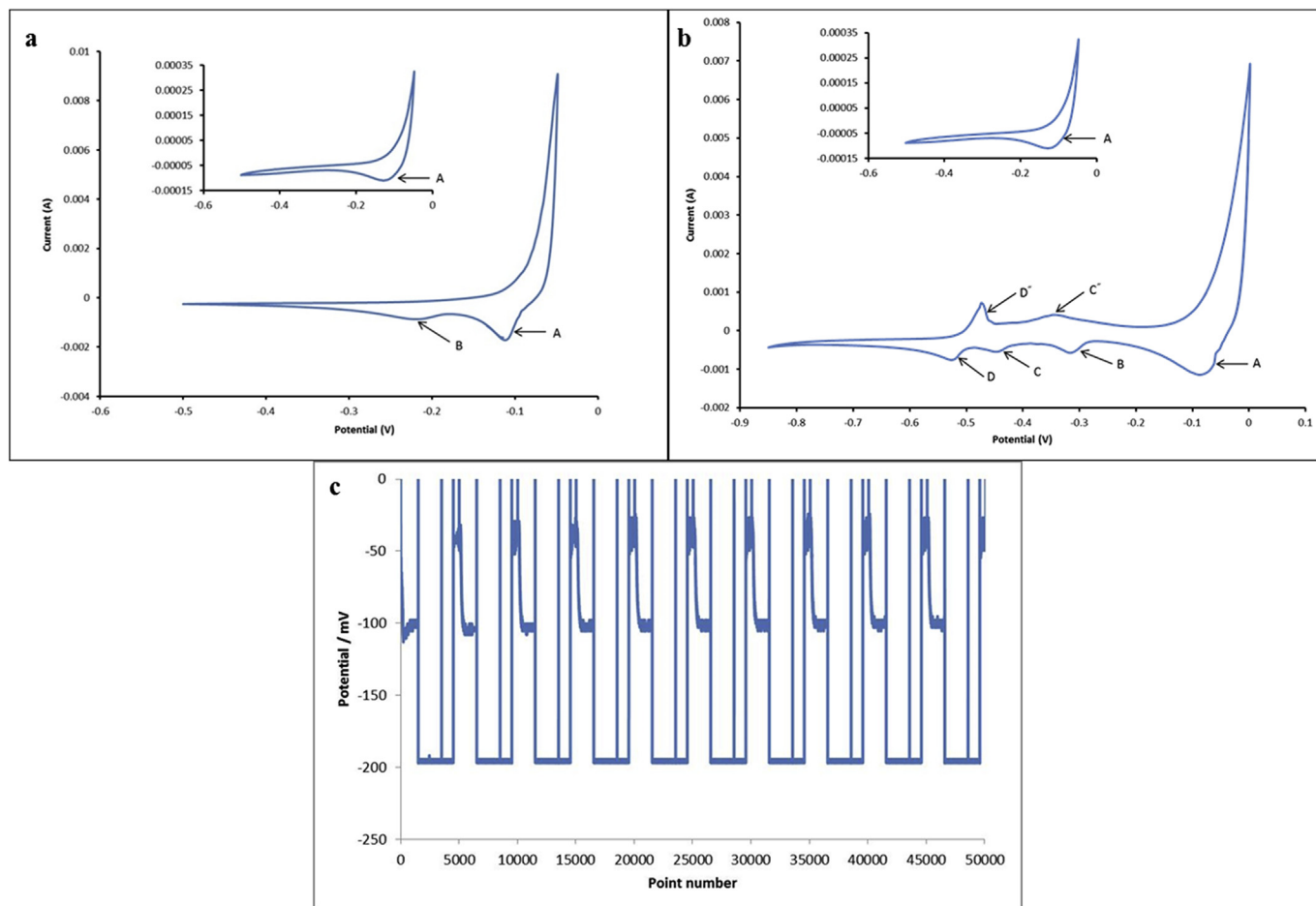
Fig. 1. (a) Cyclic voltammogram for Cu foil electrode in 1 mM $BiCl_3$ in 0.5 M HCl vs. Ag/AgCl. Insert: Cu foil electrode in 0.1 M HCl, at a scan rate of 10 mV s^{-1}; (b) Cyclic voltammogram of Cu foil electrode in 1 mM $SnCl_2$ in 0.1 M HCl vs. Ag/AgCl. Insert: Cu foil electrode in 0.1 M HCl, at a scan rate of 10 mV s^{-1}; (c) E-ALD cycle of Bi deposition on Cu foil.

CV of 0.1 M $BiCl_3$ in 0.5 M HCl is also shown in Fig. 1 (a). It showed two reduction peaks at -0.1 V (A) and -0.2 V (B). The former peak is a characteristic of a Cu substrate that is also found in the Cu substrate CV. The latter peak is associated with Bi UPD with an onset UPD potential of -0.15 V, and beyond -0.5 V hydrogen evolution starts. The UPD stripping peak is not visible, indicating that the oxidation of Bi does not occur. This is caused by the dissolution of Cu occurring first and depolarising the electrode. The same phenomenon was reported using the deposition of Sb on Cu in chloride solutions [31]. Fig. 1 (b) shows the CV of 0.1 M $SnCl_2$ in 0.1 M HCl, four reduction peaks at -0.1 V (A), -0.3 V (B), -0.43 V (C) and -0.51 V (D). These were due to the Cu substrate, and the preceding three peaks were from Sn species. The peak at -0.43 V was assigned as the Sn UPD and the other two peaks indicated bulk alloy formation. Two oxidation peaks of Sn species were found at -0.48 V and -0.35 V, corresponding to bulk Sn stripping and UPD Sn stripping, and hydrogen evolution occurred beyond -0.85 V. A study of Sn deposition on Au (100) reported a similar observation, namely that the deposition of Sn occurs in three stages involving the UPD deposition, surface alloy deposition and bulk alloy deposition [32].

3.1.2. Electrodeposition studies

3.1.2.1. Bi thin films. Bi thin films were synthesised by the deposition of $BiCl_3$ at UPD potential using a cycle that was repeated up to 300 times to grow the film. The potential and point number plot for the first 10 cycles is shown in Fig. 1 (c). The cycle used was made up of the following steps: (i) Pump $BiCl_3$ for 15 s, (ii) Deposit $BiCl_3$ at -200 mV for 10 s (no solution pump), (iii) Rinse with 0.1 M HCl at -200 mV for 5 s and (iv) Rinse with 0.1 M HCl at OCP for 5 s. Fig. 2 (a–d) shows the morphology of the formed material where very thin hexagonal structures were obtained and no ordered packing was observed. The formed films contained bismuth, as shown on the spectra in Fig. 2 (e–f), and were evenly distributed on the surface, as shown on the EDS map.

The crystal features of the prepared Bi thin films were investigated using XRD. The XRD spectrum in Fig. 2 (g) displayed the pattern for Cu foil substrate; Bi on Cu foil deposit with the assigned peaks and the matched spectra is shown in Fig. 2 (h). The pattern for Cu can be indexed to the cubic structure of Cu (ICDD 00-004-0836); diffraction peaks at angles 38.9, 43.6, 50.2, 66.0 and 74.5 correspond to 111, 200 and 220 reflections of Cu. These diffraction peaks were also found to occur at the same diffraction angles on the Bi deposit. The diffraction peaks were assigned by matching the pattern with reference database using High-Score Plus and PDF4 file 2015, as shown in Fig. 2 (h). The diffraction peaks were further identified using the reference patterns of monoclinic copper oxide (ICDD 01-089-5899), hexagonal bismuth (ICDD 01-070-5673) and monoclinic bismuth oxide (ICDD 01-079-6670, ICDD 01-079-6671, ICDD 01-079-6672, ICDD 01-079-6673, and ICDD 00-014-0699).
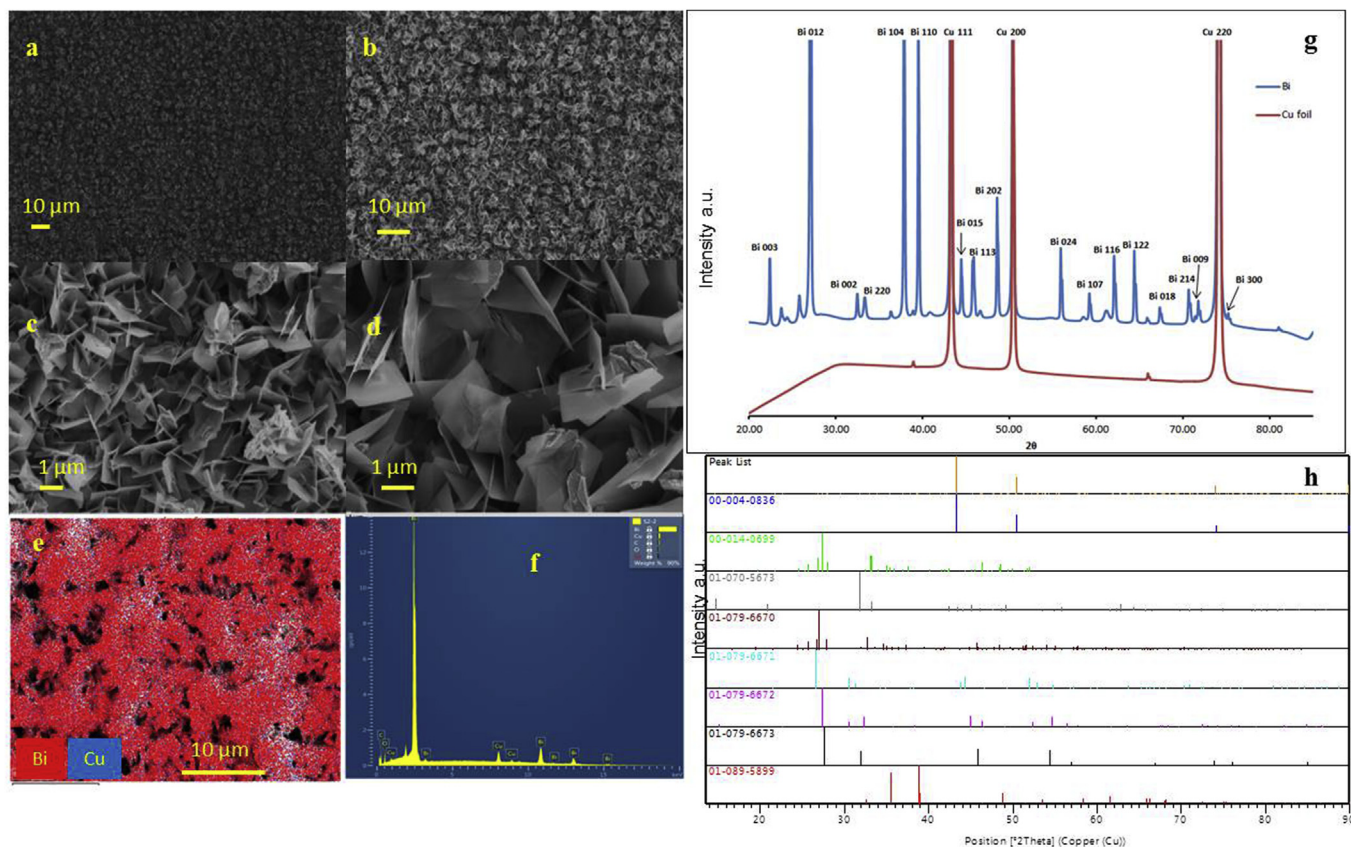
Fig. 2. (a–d) Images of electrodeposited Bi for 300 cycles; (e–f) EDS map and spectra of Bi on Cu foil deposit; (g–h) XRD spectra of Bi thin films.

3.2. Effect of deposition potential on Bi thin films

Bi deposition potential was varied along the UPD region in order to investigate the effect it has on the deposition of the thin films. BiCl$_3$ was deposited at −0.15 V, −0.2 V, −0.25 V and −0.3 V potentials using a single deposition cycle, followed by LSV measurements from a 0.5-M HCl solution. The charge associated with each potential deposition was obtained from integrating the area under the peaks. All the peaks shifted to more negative potential values with respect to the UPD used, with the materials deposited at −0.2 V and −0.25 V showing the largest potential shift as well as higher current, as shown in Fig. S1 (Supporting information). This indicates that the formed Bi layer is strongly bound to the Cu substrate and therefore will be reduced at more negative potentials. The films deposited at a potential of −0.15 V and 0.3 V were found to have the lowest potential shift and low current. The largest peak was found when the deposition was done at −0.2 V, and this shifted to −0.33 V during LSV measurements. The relationship between the charge and potential is shown in Fig. 3 (a). The charge increased from −0.15 V to −0.2 V and then decreased at −0.25 V. The optimum was found to be at −0.2 V. Well defined structural features with very thin hexagonal structures and large particles were formed at −0.2 V (c-d) as shown in Fig. 4. Increasing the potential to −0.25 V (e-f) and −0.3 V (g-h) resulted in the formation of larger more defined and well-structured particles. The small thin structures observed at −0.2 V disappeared. Smaller particles were present at less negative potentials (−0.15 V - (−0.2 V)), while low nucleation rate occurred at positive potentials generating coarse particles. The opposite occurred when the potential was more negative (−0.25 - (−0.3 V)), where larger particles formed due to the high rate of nucleation. This was also found to occur when Gao et al. [10] electrodeposited SnBi from a deep eutectic solvent. This study also reported that Bi deposition potential influences the Bi content of the formed SnBi deposit. Bi-electrodeposited films usually contain dendrites, which are very easy to form when deposition is done without additives [14]. Dendrite presence is favoured by grain nucleation. In this work, the lack of dendrites in the formed Bi films indicated that the deposition occurred by growth of already deposited crystals, which explains the stacking of crystallites observed in the SEM micrographs.

The EDS map in Fig. 5 (a–c) and spectra in Fig. 5 (d) further confirmed the distribution of the deposit across the surface and the presence of Bi. The XRD pattern in Fig. 5 (e) further confirms that the deposit at −0.2 V was slightly different to the other deposits. The pattern for the −0.2 V deposit had additional peaks at angles of 25.98, 36.40 and 41.10, corresponding to Bi. The peaks at −0.2 V were well resolved in contrast to the other deposition potentials, as indicated on the graph by Bi (002) and Bi (220) peaks.

3.2.1. SnBi thin films

SnBi thin films were deposited at UPD potentials of Sn and Bi, as can be concluded from the CV curves shown in Fig. 1 (a & b). Sn deposition was further investigated by the deposition of Sn at −0.48 V onto Cu foil and conducting an LSV scan to reduce the Bi from the electrolyte solution. The presence of Sn is evident from the appearance of the reduction peak at −0.32 V (Fig. S2). Further experiments were done to determine the deposition of Sn at potentials of −0.35 V, −0.4 V, −0.45 V and −0.55 V. The relationship
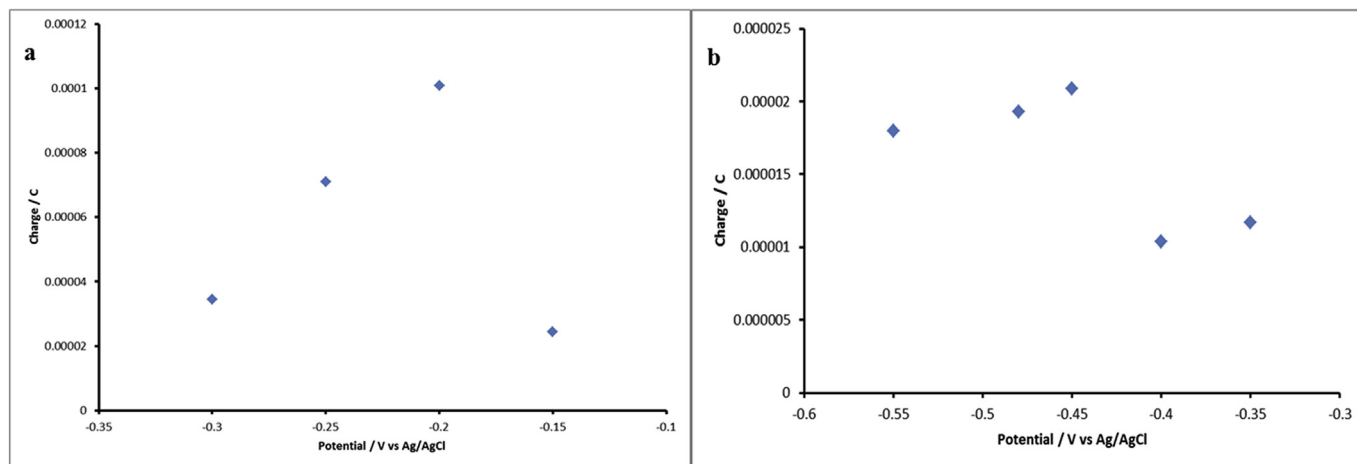
Fig. 3. (a) Charge and potential plot of Bi deposition at various potentials within UPD region; (b) Charge and potential plot of Sn deposition at various UPD potential.

between the charge and each potential is shown in Fig. 3 (b). It was found that the maximum deposition of Sn occurs at −0.45 V.

The combination of the above information on Sn deposition and the investigation of Bi deposition on Cu foil were used to formulate a deposition cycle for both elements. Bi has been successfully deposited at UPD on Cu foil; the next step was the introduction of a Sn deposition step. The deposition of the Sn layer step first followed by Bi would not work because of the surface replacement reaction of Sn by Bi. Therefore, the first layer of Bi needed to be deposited. Using the open circuit potential of −0.05 V to rinse in between the depositions of each element resulted in no film growth. This is due to the dissolution of Cu oxide in the electrolyte, which causes a change in the open circuit potential over time, as explained in Section 3.1.1. Therefore, the potential needed to be controlled until both layers had been deposited. The deposition cycle used was made of the following steps: (i) Flow Bi for 15 s, (ii) Deposit Bi at −200 mV for 10 s, (iii) Pump Sn at −480 mV for 15 s, (iv) Deposit Sn at −480 mV and (v) Rinse with 0.1 M HCl at OCP for 15 s. The first 10 cycles used are shown in Fig. S3. Bi was deposited at −200 mV, where a higher Bi content was obtained. Bi preferentially deposits over Sn, hence slight lowering of the potential was done to give the Sn deposition a competitive edge or to favour the deposition of Sn. Parameters including the deposition potential of Bi and the concentration of Sn were investigated for their effect on the structure and morphology of the films.

The morphology of the SnBi thin films was investigated using SEM microscopy and the obtained images are shown in Fig. 6 at different magnifications. The film showed thin sheet-like material and agglomeration was observed. It contained both Sn and Bi distributed across the surface, showing that the material is made up of both elements, as shown by the EDS map in Fig. 6 (e−h). The crystal structure was determined using X-ray diffraction pattern, shown in Fig. 6 (i & j). The XRD pattern of SnBi thin film was overlaid with that of Bi material and Cu foil substrate. The diffraction peaks were assigned by matching the pattern with reference database using High-Score Plus and PDF4 file 2017, as shown in Fig. 6 (j). The diffraction peaks were identified from the reference patterns of Cu (ICDD 00-004-0836), Bi (ICDD 01-070-5673), BiSn (ICDD 00-076-7574, ICDD 00-076-7575), $Bi_{1.2}Sn_{0.2}$ (ICDD 01-082-9505), $Bi_2Sn_2O_7$ (ICDD 00-056-0646), CuSn (IDCC 00-006-0621), Cu_6Sn_5 (ICDD 00-045-1498, ICDD 01-081-8261) and SnO (ICDD 00-007-0195). The peaks at angles 26.9, 28.7, 32.8, 33.5, 53.3 and 54.3 were assigned to Sn 200, 101, 220, 211, 301 and 400, respectively.

There was a slight shift and broadening of Cu foil peaks observed on the SnBi film on Cu foil. The Bi peaks were also found to have shifted, while new peaks were identified. The Bi peaks shifted to the lower diffraction angles, while those of Cu broadened. The d-spacing of possible reflections of the prepared SnBi and Bi films based on Bi 012 were found to be 3.008 Å and 3.263 Å, respectively, based on Rietveld refinement data. The shifting of the 012 Bi peaks and the presence of other phases of the SnBi, including $Bi_{1.2}Sn_{0.2}$, indicates that an alloy was formed. The formation of intermetallic Cu−Sn phases (CuSn, Cu_6Sn_5) during electrochemical alloy deposition is better explained through the findings of a study by contact immersion deposition of Sn onto Cu [33]. This work showed that the growth mechanism involves (i) the formation of an Sn monoatomic layer on the Cu surface at UPD, (ii) the exchange of site between Cu and UPD deposited Sn, resulting in Cu atoms moving into the surface (this becomes the nuclei of Cu−Sn intermetallic phases) and (iii) the following UPD layer of Sn on Cu then forming the Cu−Sn intermetallic layer. The diffusion of Sn and Cu atoms through the alloy layer limits the growth rate of Cu−Sn intermetallic phases. Intermetallic phases were also found when Sn and Bi layers were electrodeposited on reflowed SnBi solder alloys using a Cu substrate [34]. Lee and Goh [34] found that a layer of Cu_6Sn_5 forms at room temperature. According to their study, the growth mechanism explained above for Cu−Sn formation does not occur when Bi is deposited as the first layer, which is contrary to our findings [34]. It is important to note that the method used was bath deposition in methane sulphonic and citric acid-based, and not a potential controlled or UPD method. The presence of intermetallic Cu−Sn phases reported in this study indicates that the first layer of Bi did not cover the entire surface or left space within the monoatomic layer for the diffusion of Cu atoms. Electrodeposition of SnBi coatings on Cu foil from deep eutectic solvent was able to produce films that contained phases of Sn, Bi and Cu substrate and no trace of other intermetallic phases [10].

3.3. Effect of Sn concentration on morphology of SnBi thin film

The concentration of Sn was varied, while the Bi was kept constant to investigate the effect it had on the formed film. The Sn concentration ratios in SnBi of 10:1, 5:1, 4:1, 3:1, 2:1 and 1:1 were used to form deposits for 100 cycles. The morphology of the SnBi films formed at different concentrations of Sn is shown in Fig. 7(a−f). Well-defined structures with larger particles were
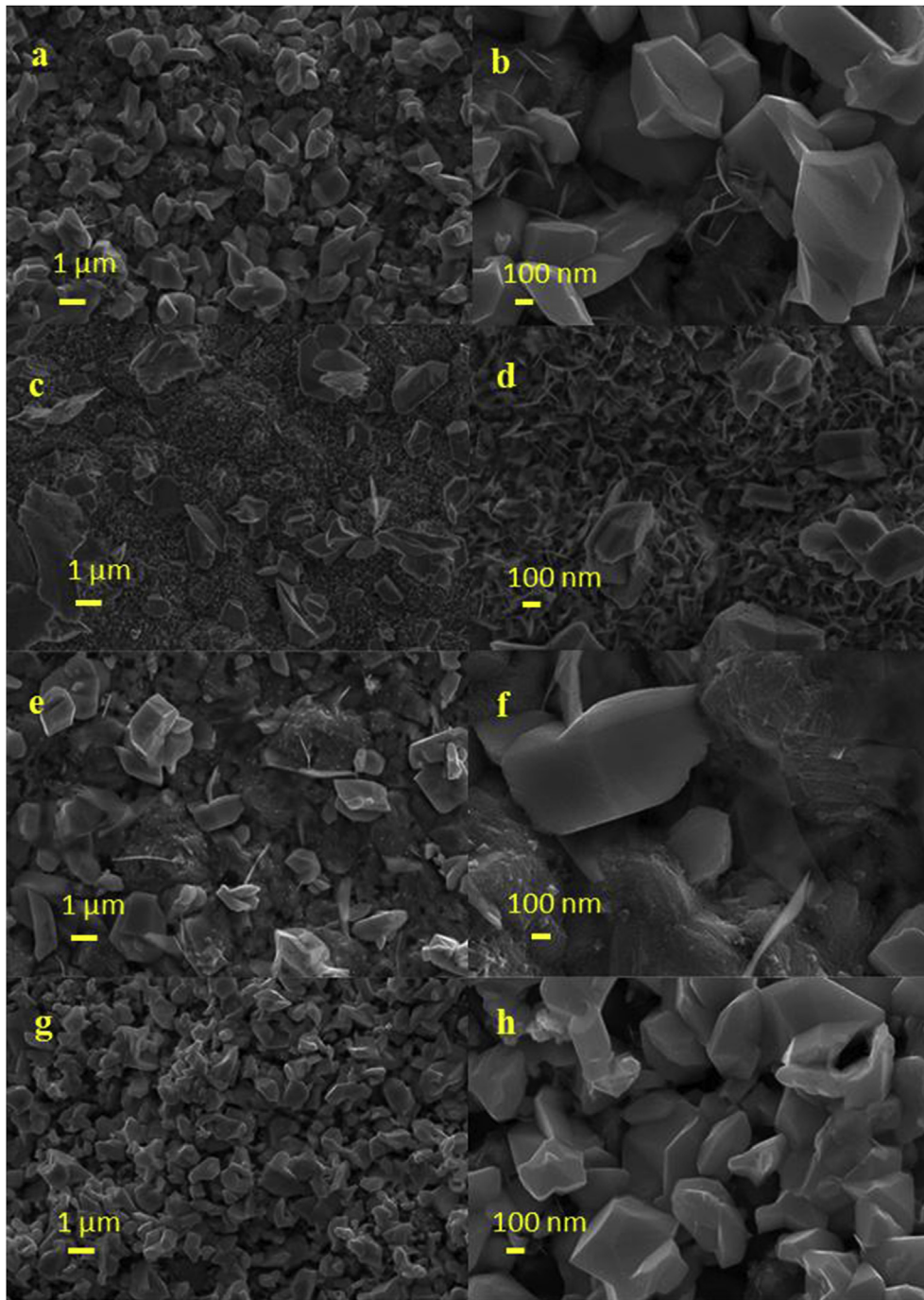
Fig. 4. Electrodeposited Bi at −0.15 V (a−b), −0.20 V (c−d), −0.25 V (e−f) and −0.30 mV (g−h) for 100 cycles.

obtained when Bi and Sn ratios were the same, while increasing the concentration of Sn resulted in smaller, thin, sheet-like particle formation.

The deposition behaviour of Sn and Bi affects the structural features of the formed deposit. SnBi deposits can form by growth of already deposited crystallites or nuclei formation [14]. The morphology of the SnBi films indicated that deposition occurs by both mechanisms where the stacked particles are a result of particle growth on already existing deposits. They grow up to a certain point until the conditions are favourable for new nuclei formation. These two growth mechanisms result in the observed grove-like or excavated shape on the surface. Modification of deposition solution or the total concentration of the precursor metal ions as observed during a study on the control and microstructure of SnBi alloys affects the structure of the material [14]. This study found that when the SnBi ratio in a solution is 1:1, uniform polyhedral crystallites deposits were formed. Increasing the concentration of Sn resulted in less structurally defined particles due to the simultaneous occurrence of hydrogen evolution and SnBi deposition. The difference in grain sizes indicates that the formation of SnBi is dependent on the composition of the precursor solution (amount of Sn and Bi in the precursor solutions).
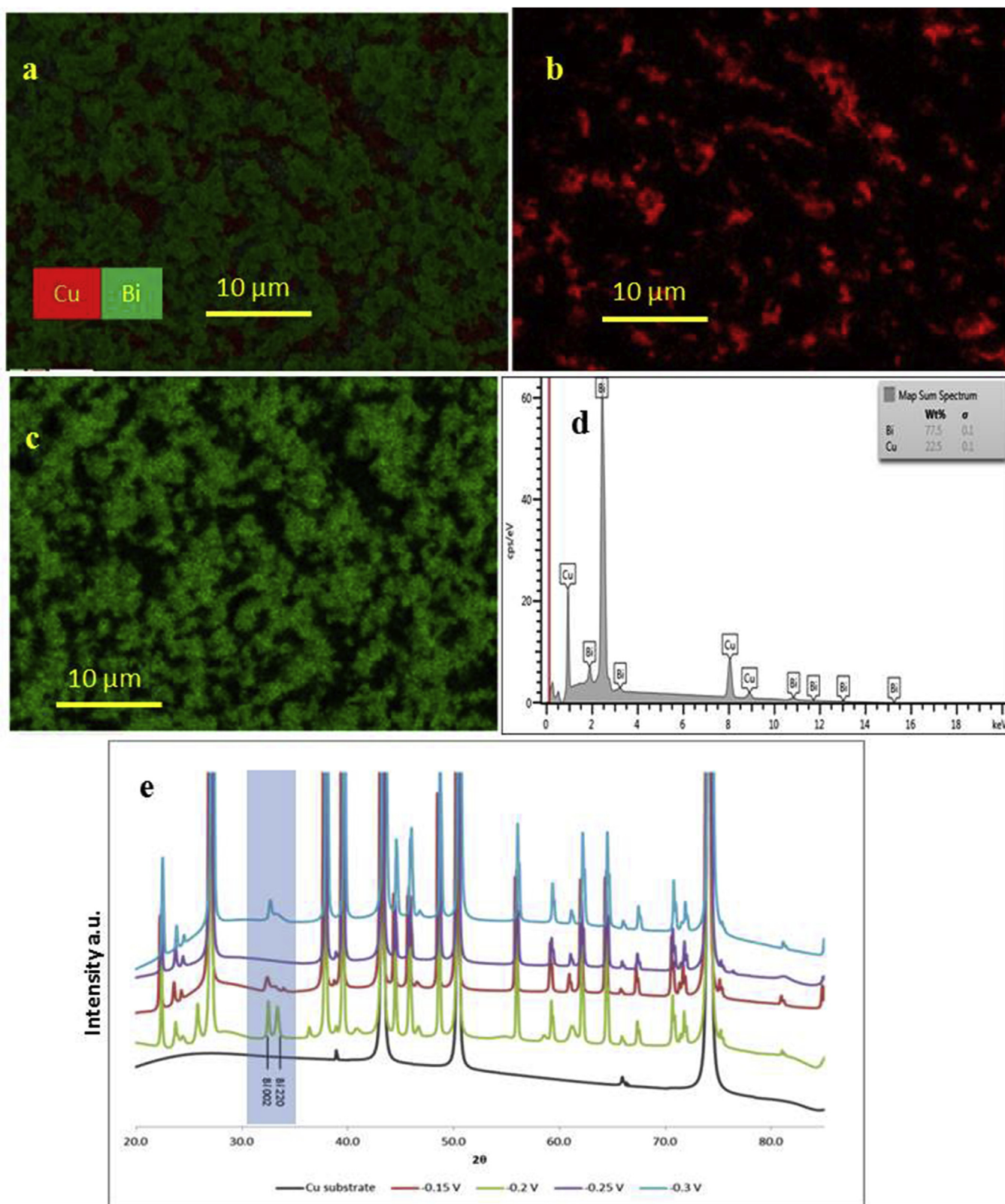
Fig. 5. (a−c) EDS map for electrodeposited Bi films with at −0.15 V for 100 cycles; (d) EDS spectra for electrodeposited Bi at −0.15 V for 100 cycles; (e) XRD pattern for Bi on Cu foil at varied potentials.
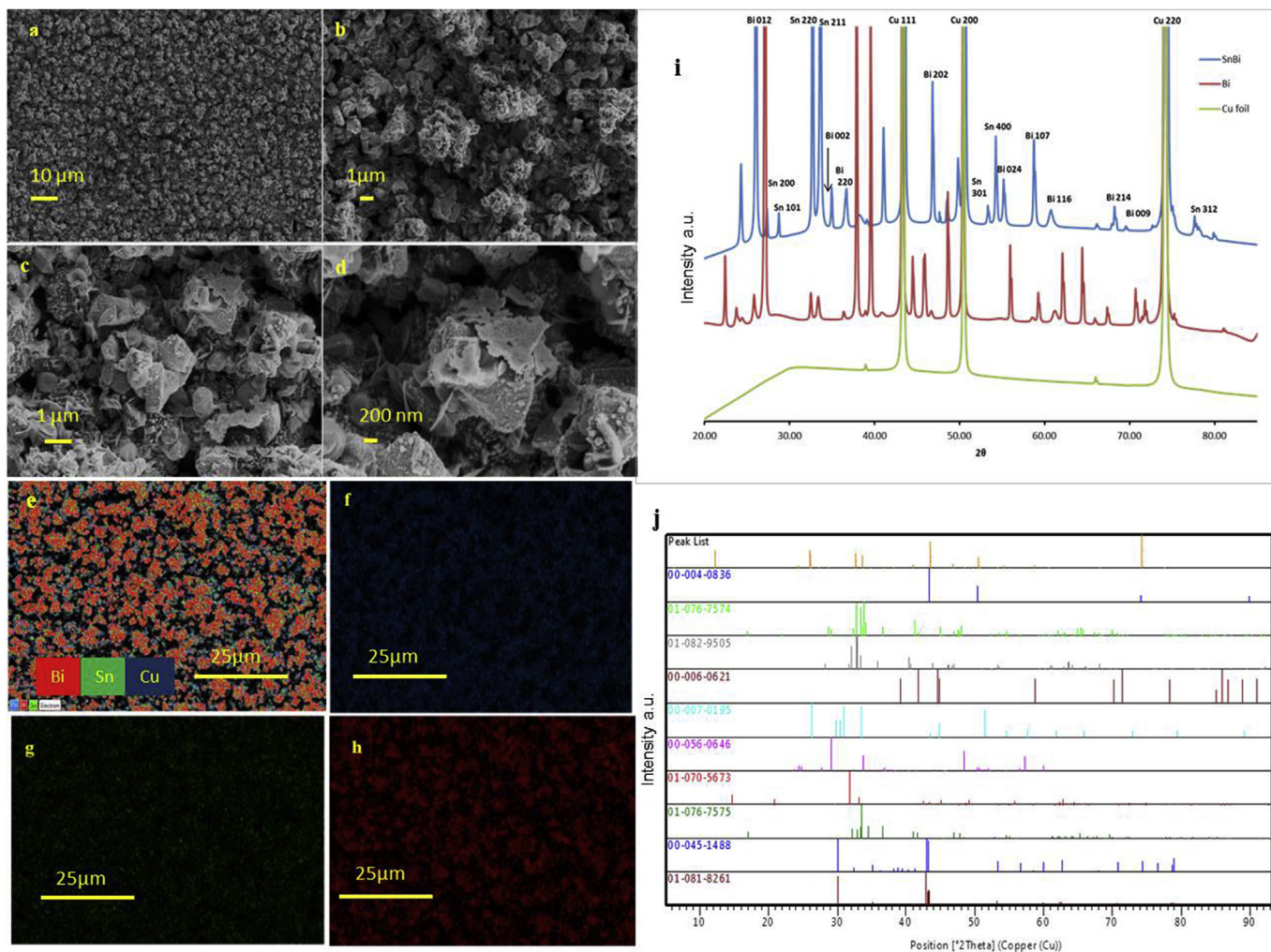
Fig. 6. (a–d) Images of electrodeposited SnBi thin films for 300 cycles; (e–h) EDS map for the SnBi thin films; (i) XRD spectra of SnBi thin films; (j) Matched XRD spectra of SnBi thin films.

The presence of Sn and Bi was further confirmed using the EDS map shown in Fig. 8 (a–d) and the spectra in Fig. 8 (f). The elemental map showed that both Sn and Bi were distributed evenly over the surface. Further structural differences were investigated using XRD. The pattern for all the different concentrations is shown in Fig. 8 (e). Diffraction peaks appeared at parallel angles for different ratios, indicating that materials were crystalline with similar structural patterns.

The elemental composition of the deposits was confirmed using ICP-MS, as summarised in Table 1. The highest amount of 0.3589 mg Bi was obtained when using a ratio of 1:1 for Sn:Bi, while Sn was found to be 0.0004511 mg at this ratio. The highest Sn content of 0.005481 mg was obtained for a 10:1 SnBi ratio, while Bi content at this ratio was 0.1162 mg. Bi content decreased with the increase in Sn content, and vice versa, even though the Bi content remained much higher than that of Sn. Half the amount of Bi was obtained when the concentration of Sn was doubled based on the ratio of 1:80 for SnBi (1:1) and 1:40 for SnBi (2:1). Further increase in Sn content decreased Bi content to as low as 1:21 for SnBi (10:1). Increasing the concentration of Sn was able to effectively decrease the content of Bi in the deposit formed due to the competitive nature of Sn and Bi deposition [10]. Bi content in the deposit will be

higher than Sn due to Bi being much nobler than Sn and because Bi has a higher atomic mass than Sn (208 vs. 118 g/mol) [14]. Efforts to increase Sn content in the SnBi deposit have involved the use of additives such as polyethylene glycol to inhibit Bi deposition, thereby increasing Sn deposition and content [14,35,36]. Suh et al. [37] investigated the effects of plating conditions on the composition and microstructure of an SnBi electrodeposit using a methane sulphonate bath. They also report similar observations, where increasing the Sn content in the bath (solution) increased the content of Sn in the deposits. Similar observations were found for the electrodeposited SnBi coatings from a deep eutectic solvent on a Cu foil substrate [10]. Tsai also found a higher Sn content when the bath Sn concentration was increased in 10 times compared to that of Bi in the same solution [14].

The thickness of the deposit was investigated and the cross-sectional images for a 300-cycle deposit are shown in Fig. 9 (a–d). The 300-cycle material was found to be 2 μm thick and it slightly varied along the deposit. This variation is associated with the material growing into a rough Cu substrate. The use of a single-crystal Cu substrate would result in better-quality films. Laminar flow also needs to be established earlier in the flow channel during deposition to eliminate uneven growth. XRD patterns confirmed
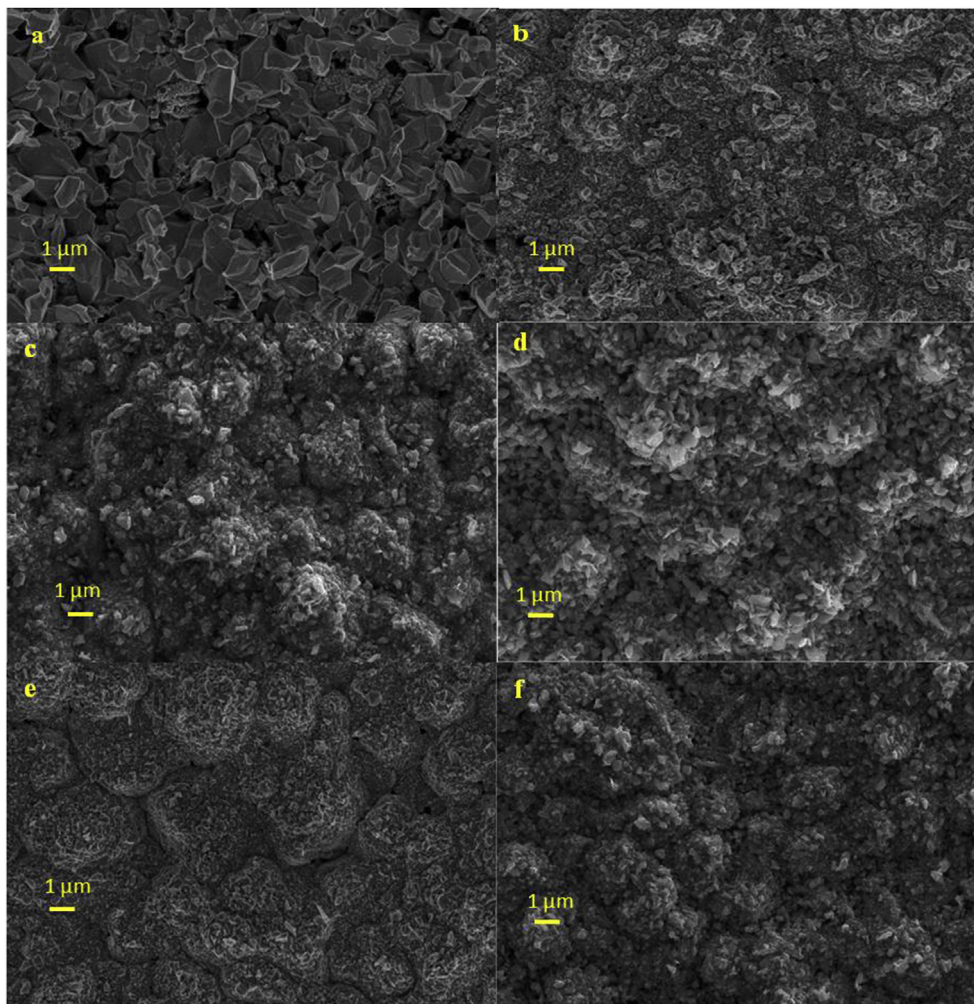
Fig. 7. Electrodeposited SnBi films of ration 1:10 (a), 1:5 (b), 1:4 (c), 1:3 (d), 1:2 (e), 1:1 (f) for 100 cycles.
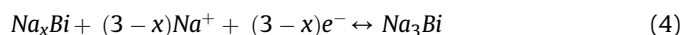
that Sn was alloying with the substrate, forming CuSn intermetallic phases by diffusion of Sn and Cu atoms. The elemental analysis performed on the cross-sections in Fig. 9 (e−h) showed that both Sn and Bi were present; Sn was evenly distributed across the material, while Bi was predominantly found on the surface.

3.4. Electrochemical tests for sodium ion batteries

3.4.1. Electrochemical performance of SnBi electrodes

The CV analyses of SnBi (1:1) and SnBi (3:1) are shown in Fig. 10 (a & b), cycled at a scan rate of 0.1 mV s^{-1} in the voltage range of 0.005−1.5 V. The first cathodic curves of SnBi (1:1) and SnBi (3:1) presented four reduction peaks at ~ 1.4, 1.0, 0.6 and 0.4 V. The peaks at 1.4 V and 1.0 V in the first cycle disappeared in the next cycles as a result of solid electrolyte interface (SEI) film formation. The peak at 0.6 V corresponds to the sodiation of Na_3Bi and $NaSn_3$ [38,39]. The strong peak at 0.4 V identifies Na_xBi and Na_9Sn_4 [22,38,39]. The first anodic peaks at 0.8 and 0.7 V belong to desodiation of Sn and Bi, which is well matched with the literature [38,39]. During the subsequent cathodic cycles, the peaks are slightly shifted to the positive side and the peak at 0.4 V is split into two peaks occurring at 0.37 and 0.31 V. During the following anodic cycles, the desodiation peaks are slightly shifted to the positive side and the peaks at 0.8 and 0.7 V are split into two peaks. The redox reactions in SnBi samples should be observed by following equations (3)−(6). The

reduction peak at ~0.4 V has a characteristic small shoulder peak, and this peak is more pronounced in the CV curve for SnBi 3:1 (Fig. 10 (b)). This peak could be due to the presence of Sn, as it suffers more volumetric changes during cycling, segregates and fails to intercalate Na, resulting in capacity fade [4].

$$Bi + xNa^+ + xe^- \leftrightarrow Na_xBi \tag{3}$$

$$Na_xBi + (3-x)Na^+ + (3-x)e^- \leftrightarrow Na_3Bi \tag{4}$$

$$3Sn + Na \leftrightarrow NaSn_3 \tag{5}$$

$$4a - NaSn + 5Na \leftrightarrow Na_9Sn_4 \tag{6}$$

To understand the electrochemistry of the SnBi (SnBi (1:1) and SnBi (3:1)) materials further, galvanostatic cycling analysis was performed within the voltage range of 0.05−1.5 V at 0.1C (38.5 mA g^{-1} based on the Bi theoretical capacity 1C = 385 mAh g^{-1}, because Bi content is higher than Sn content according to the ICP data in Table 1). The first discharge curves show four plateaus at 1.1 V, 0.67 V, 0.5 V and 0.36 V, and the first charge curves at 0.8 V, 0.75 V, 0.65 and 0.6 V for both samples SnBi (1:1) and SnBi (3:1). These redox peaks were consistent with the CV analysis (Fig. 10 (a) and (b)). The peak at 1.1 V disappears during the following cycles, which could be due to the formation of the SEI layer and
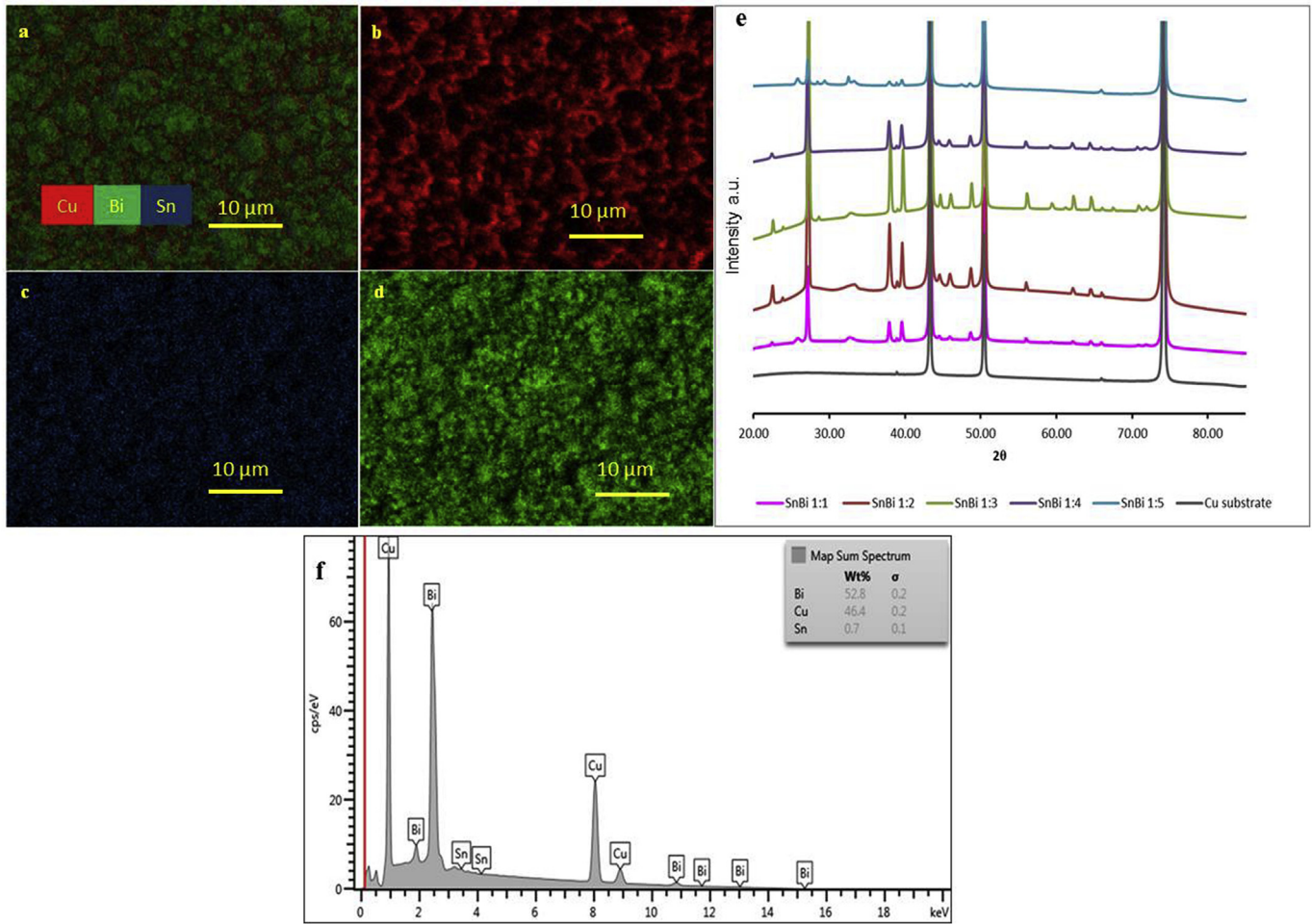
Fig. 8. (a−d) EDS map for electrodeposited SnBi films with a ratio of 1:2 for 100 cycles; (e) XRD pattern for electrodeposited SnBi films with a various Sn distribution in solution; (f) EDS spectra for electrodeposited SnBi films with a ratio of 1:3 for 100 cycles.

Table 1
Summary of SnBi content from ICP-MS analysis.

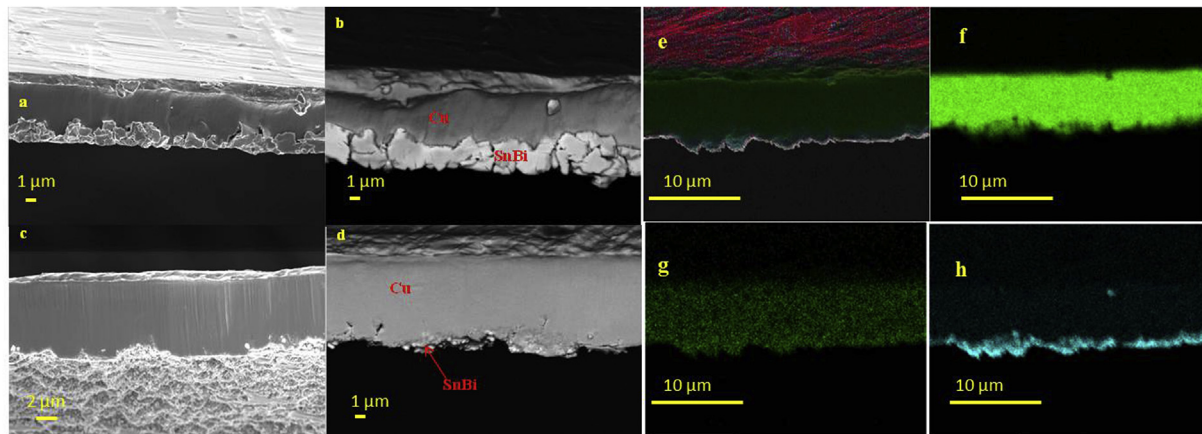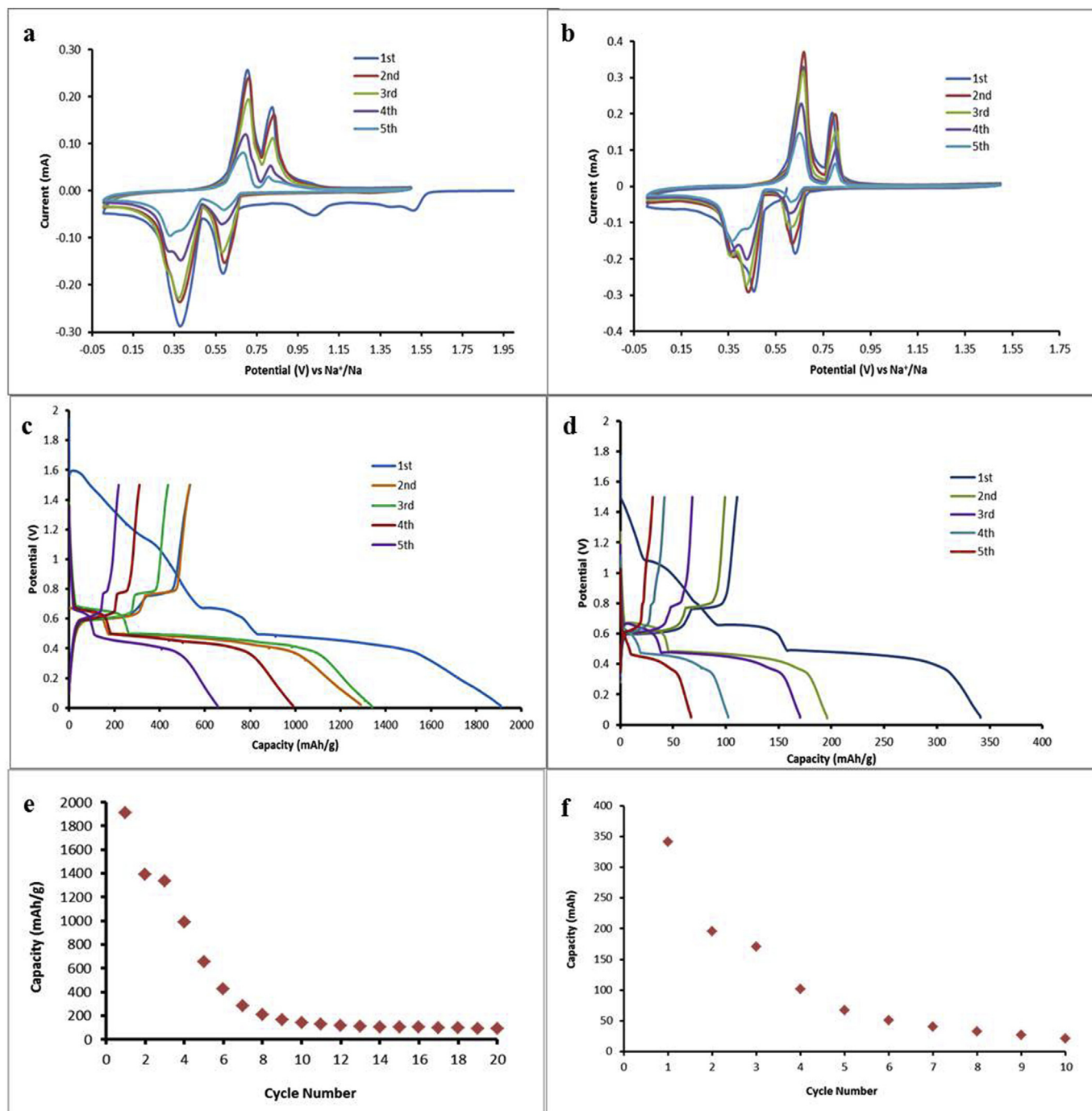| SnBi ratio in solution	Sn in the deposit/mg	Bi in the deposit/mg	Sn:Bi ratio after deposition
1:1	0.004511	0.3589	1:80
3:1	0.004471	0.1808	1:40
5:1	0.003443	0.1190	1:34
10:1	0.00581	0.1162	1:21

Fig. 9. (a−d) Thickness of 300 cycle SnBi Deposit; (e−h) EDS map of SnBi Deposit 300 cycle deposit.

Fig. 10. Discharge and charge profiles of (a) SnBi (1:1), (b) SnBi (1:3) for the first five cycles at 0.1C (38.5 mA g^{-1}) within 0.05–1.5-V range. Cyclic voltammogram of (c) SnBi (1:1), (d) SnBi (1:3) electrode at a scan rate of 0.1 mV s^{-1} within the potential range of 0.05–1.5 V vs. Na$^+$/Na. Cycling performance of (e) SnBi (1:1), SnBi (1:3) (f) electrode at 0.1C (38.5 mA g^{-1}) within 0.05–1.5-V range.

irreversible reactions. These plateaus occurred between the 0.2 and 1.0 V region, indicating that this is where the sodiation/desodiation reaction of Na$_x$Bi and Na$_x$Sn occurs [12]. These reactions are reversible, as similar plateaus were found on both discharge and charging curves [38,40]. The first discharge and charge capacity of 1900 and 533 mAh g^{-1} were observed for SnBi (1:1), while the SnBi (3:1) showed first discharge and charge capacity of 341 and 111 mAh g^{-1}. The second-cycle discharge capacity of 1307 and 196 mAh g^{-1} for SnBi (1:1) and SnBi (3:1) respectively was observed. However, SnBi (1:1) exhibits high initial irreversible capacity loss (ICL)

of 593 mAh g^{-1} compared to that of SnBi (3:1) (ICL = 145 mAh g^{-1}), which is around 2.3 times higher than the theoretical capacity of Sn (847 mAh g^{-1}) and around 5 times higher than the theoretical capacity of Bi (385 mAh g^{-1}). The increased first discharge capacity is mainly due to the SEI film formation and partial sodiation of Sn and Bi, which overlap during the electrochemical reaction [38]. The initial discharge capacity was found to decrease rapidly in the subsequent cycles until a capacity of 659 mAh g^{-1} and 67 mAh g^{-1} at the fifth cycle for SnBi (1:1) for the SnBi (3:1) electrodes, respectively. When comparing the two electrode materials, it was

Table 2
Comparison of the electrode materials electrochemical performance.

	SnBi (1:1)		SnBi (3:1)	
Initial discharge capacity (mAh g^{-1})	1900		338	
Second cycle (mAh g^{-1})	1297		195	
Fifth cycle (mAh g^{-1})	633		67	
Tenth cycle (mAh g^{-1})	140		22	
Discharge plateau (V)	0.5	0.67	0.6	0.76
Charge plateau (V)	0.5	0.67	0.6	0.76

Table 3
EIS measurement of Bi-based electrodes.

Electrode	R_s (Ω)	R_f (Ω)	R_{ct} (Ω)
SnBi/Cu foil (1:1)	14.16	12.69	326
SnBi/Cu foil (3:1)	7.37	2.15	55
Bi/CFC	4.28	23.32	473
Pure Bi powder	17.42	10.2	986

found that SnBi (1:1) had a much higher initial discharge capacity than SnBi (3:1). The former was also able to retain capacity for a longer period of 100 cycles (38 mAh g^{-1}), while the latter crashed much earlier at the 12th cycle (1.8 mAh g^{-1}) and zero until the 20th cycle. Similar studies reported an initial discharge capacity of 1013 mAh g^{-1} at 40 mA g^{-1} for bismuth on graphene nanocomposite and 310 mAh g^{-1} for a bare bismuth electrode [39].

The cycling performance of the SnBi 1:1 electrode is shown in Fig. 10 (e). The graph shows that the initial capacity of 1900 mAh g^{-1} drops rapidly to 140 mAh g^{-1} within 10 cycles and continues to drop until 60 mAh g^{-1} at 50 cycles until it reaches 35 mAh g^{-1} at 100 cycles, while the cycling performance of SnBi 3:1 (Fig. 10 (f)) showed a rapid capacity loss within the first 10 cycles to 20 mAh g^{-1} and then to zero on cycle number 10. The capacity fade showed that the material is unstable. The redox pairs were slightly shifted for the two electrodes while the charge and discharge plateau remained the same, as shown in Table 2. The CV curves for both electrodes resembled that of a pure Bi electrode material and the charge and discharge plateaus matched those of the pure Bi electrode tested by Su et al. [12]. From the obtained results, Bi was found to be the dominant material. Previous studies show that Sn charge and discharge curves contain four plateaus that become less distinct with cycling; usually three are visible, which is not the case on this material [4,8].

The SnBi electrode has considerable potential as an anode material for Na-ion batteries. This is demonstrated by comparing it with similar materials from literature [3]. The Nyquist plots of the SnBi (1:1) and SnBi (3:1) electrodes are shown in Fig. 11 (a) and (b). The Nyquist plots were fitted using the electrical circuit (inset Fig. 11 (a) and (b)) and the fitted parameters of the samples, and the comparison to other Bi electrode is shown in Table 3. The SnBi (1:1) and SnBi (3:1) electrode had R_{ct} of 326 Ω and 55 Ω, and an R_f value of 12.69 Ω and 2.15 Ω, respectively. These findings indicate that the

film with lower film and charge transfer resistance should give a higher capacity, which was contrary to what was obtained, as the SnBi (3:1) presented lower capacity. Liu et al. [41] synthesised bismuth nanosheets on carbon fibre cloth (Bi/CFC), which is a self-supported electrode material. This material was found to exhibit excellent properties with an R_{ct} of 473 Ω; they also reported that of Bi powder found to be 986 Ω. These values are much higher than that obtained for SnBi (1:1) and SnBi (3:1) electrode, indicating that our material is good for Na storage, but lacks capacity retention and stability. The Bi/CFC was found to be much more stable and was able to maintain a much higher capacity over 100 cycles. Nevertheless, SnBi on Cu foil electrode lacks the support that CFC provides to enhance stability caused by volumetric expansion during cycling.

4. Conclusion

Microstructured thin films of Bi and SnBi were fabricated using E-ALD on a Cu foil substrate. Parameters including the deposition potential of Bi and the concentration of Sn were investigated for their effect on the structure and morphology of the films. The UPD potential of Sn was found to be −0.48 V and that of Bi was −0.2 V. These were used to develop a cycle for deposition of pure Bi films and for both SnBi films. Well-defined structures with larger particles were formed when Bi and Sn contents were similar. The SnBi thin film with a ratio of 1:80 was found to contain the overall high amount of Sn and Bi, while the increase in Sn concentration did not improve the amount of Sn deposited. SnBi thin films grown on Cu foil using E-ALD technique were then tested as anode for Na-ion batteries. The electrode exhibited a high initial discharge capacity and showed major capacity loss within the first 10 cycles and retained low capacity until the 100th cycle. Further investigations need to be done to improve stability during cycling, such as the introduction of carbon support material.
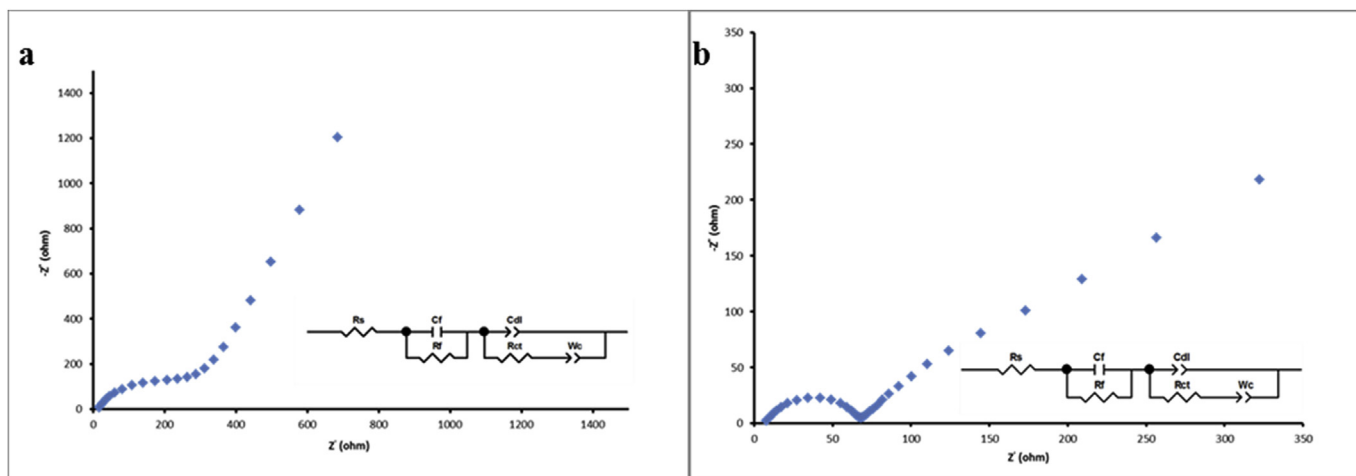
Fig. 11. Nyquist plot of the EIS of the (a) SnBi 1:1, (b) SnBi (1:3) electrode with an insert of circuit of electrode and values of the circuit components (R_s: electrolyte resistance and ohmic resistance; R_f: resistance of the SEI; R_{ct}: charge transfer resistance; C_f: surface passivating layer capacitance; C_{dl}: double-layer capacitance; W_c: Warburg impedance).

Acknowledgements

Appendix A. Supplementary data

Supplementary data to this article can be found online at https://doi.org/10.1016/j.jallcom.2019.151658.

References

[1] L.B. Sheridan, D.K. Gebregziabiher, J.L. Stickney, D.B. Robinson, Langmuir 29 (2013) 1592−1600.
[2] C.-C. Hu, Y.-D. Tsai, C.-C. Lin, G.-L. Lee, S.-W. Chen, T.-C. Lee, T.-C. Wen, J. Alloy. Comp. 472 (2009) 121−126.
[3] H. Pan, Y.-S. Hu, L. Chen, Energy Environ. Sci. 6 (2013) 2338−2360.
[4] Z. Li, J. Ding, D. Mitlin, Accounts Chem. Res. 48 (2015) 1657−1665.
[5] M. Dahbi, N. Yabuuchi, K. Kubota, K. Tokiwa, S. Komaba, Phys. Chem. Chem. Phys. 16 (2014) 15007−15028.
[6] K. Kubota, S. Komaba, J. Electrochem. Soc. 162 (2015) A2538−A2550.
[7] D. Stevens, J. Dahn, J. Electrochem. Soc. 147 (2000) 1271−1273.
[8] J. Cui, S. Yao, J.-K. Kim, Energy Storage Mater. 7 (2017) 64−114.
[9] Y.-D. Tsai, C.-C. Hu, J. Electrochem. Soc. 156 (2009) D58−D63.
[10] Y. Gao, W. Hu, X. Gao, B. Duan, Surf. Eng. 30 (2014) 59−63.
[11] Y. Zhang, S. Lu, M.-Q. Wang, Y. Niu, S. Liu, Y. Li, X. Wu, S.-J. Bao, M. Xu, Mater. Lett. 178 (2016) 44−47.
[12] D. Su, S. Dou, G. Wang, Nano Energy 12 (2015) 88−95.
[13] E. Sandnes, M.E. Williams, M.D. Vaudin, G.R. Stafford, J. Electron. Mater. 37 (2008) 490−497.
[14] Y.D. Tsai, C.C. Hu, J. Electrochem. Soc. 158 (2011) D482−D489.
[15] N. Okamoto, Y. Fujii, H. Kurihara, K. Kondo, Mater. Trans. 50 (2009) 2570−2577.
[16] B.W. Gregory, J.L. Stickney, J. Electroanal. Chem. 300 (1991) 543−561.
[17] V. Venkatasamy, M.K. Mathe, S.M. Cox, U. Happek, J.L. Stickney, Electrochim. Acta 51 (2006) 4347−4351.
[18] J.Q. Zhang, J.Y. Yang, M. Liu, G. Li, W.X. Li, S. Gao, Y.B. Luo, J. Electrochem. Soc. 161 (2014) D55−D58.
[19] A. Gichuhi, B.E. Boone, C. Shannon, J. Electroanal. Chem. 522 (2002) 21−25.
[20] D. Banga, Y.-G. Kim, J. Stickney, J. Electrochem. Soc. 158 (2011) D99−D106.
[21] D. Banga, N. Jarayaju, L. Sheridan, Y.-G. Kim, B. Perdue, X. Zhang, Q. Zhang, J. Stickney, Langmuir 28 (2012) 3024−3031.
[22] X.H. Liang, Q.H. Zhang, M.D. Lay, J.L. Stickney, J. Am. Chem. Soc. 133 (2011) 8199−8204.
[23] J.M. Czerniawski, J.L. Stickney, J. Phys. Chem. C 120 (2016) 16162−16167.
[24] J.M. Czerniawski, B.R. Perdue, J.L. Stickney, Chem. Mater. 28 (2016) 583−591.
[25] W. Zhu, J.Y. Yang, J. Hou, X.H. Gao, S.Q. Bao, X.A. Fan, J. Electroanal. Chem. 585 (2005) 83−88.
[26] L.B. Sheridan, J. Czerwiniski, N. Jayaraju, D.K. Gebregziabiher, J.L. Stickney, D.B. Robinson, M.P. Soriaga, Electrocatalysis 3 (2012) 96−107.
[27] N. Jayaraju, D. Vairavapandian, Y.G. Kim, D. Banga, J.L. Stickney, J. Electrochem. Soc. 159 (2012) D616−D622.
[28] T.S. Mkwizu, M.K. Mathe, I. Cukrowski, Langmuir 26 (2010) 570−580.
[29] N. Jayaraju, D. Banga, C. Thambidurai, X.H. Liang, Y.G. Kim, J.L. Stickney, Langmuir 30 (2014) 3254−3263.
[30] J.L. Stickney, C.B. Ehlers, J. Vac. Sci. Technol., A: Vac. Surf. Films 7 (1989) 1801−1805.
[31] L.C. Ward, J.L. Stickney, Phys. Chem. Chem. Phys. 3 (2001) 3364−3370.
[32] M. Fonticelli, R.I. Tucceri, D. Posadas, Electrochim. Acta 49 (2004) 5197−5202.
[33] Y. Fujiwara, H. Enomoto, J. Solid State Electrochem. 8 (2004) 167−173.
[34] S.F. Lee, Y.X. Goh, A. Haseeb, Ieee, Effects of stacking sequence of electro-deposited Sn and Bi layers on reflowed Sn-Bi solder alloys, in: 2012 35th IEEE/CPMT International Electronic Manufacturing Technology Symposium, 2012.
[35] Y.D. Tsai, C.C. Hu, J. Electrochem. Soc. 156 (2009) D490−D496.
[36] Y.D. Tsai, C.H. Lien, C.C. Hu, Electrochim. Acta 56 (2011) 7615−7621.
[37] M.-S. Suh, C.-J. Park, H.-S. Kwon, Surf. Coat. Technol. 200 (2006) 3527−3532.
[38] H. Yin, Q. Li, M. Cao, W. Zhang, H. Zhao, C. Li, K. Huo, M. Zhu, Nano Res. 10 (2017) 2156−2167.
[39] P.R. Abel, M.G. Fields, A. Heller, C.B. Mullins, ACS Appl. Mater. Interfaces 6 (2014) 15860−15867.
[40] M. Mortazavi, Q. Ye, N. Birbilis, N.V. Medhekar, J. Power Sources 285 (2015) 29−36.
[41] S. Liu, Z. Luo, J. Guo, A. Pan, Z. Cai, S. Liang, Electrochem. Commun. 81 (2017) 10−13.